Hindawi
Journal of Nanotechnology
Volume 2018, Article ID 8349626, 8 pages
https://doi.org/10.1155/2018/8349626

Research Article

PMMA-Assisted Plasma Patterning of Graphene

Alfredo D. Bobadilla [1,2,3,4] **Leonidas E. Ocola,** [2] **Anirudha V. Sumant,** [2] **Michael Kaminski,** [3] **and Jorge M. Seminario** [4]

[1] *Faculty of Engineering, Universidad Peruana de Ciencias Aplicadas, Surco, Lima 33, Peru*
[2] *Center for Nanoscale Materials, Argonne National Laboratory, Argonne, IL 60439, USA*
[3] *Nuclear Engineering Division, Argonne National Laboratory, Argonne, IL 60439, USA*
[4] *Department of Chemical Engineering, Electrical and Computer Engineering, and Material Sciences and Engineering, Texas A&M University, College Station, TX 77843, USA*

Correspondence should be addressed to Alfredo D. Bobadilla; alfdoug@gmx.com and Jorge M. Seminario; seminario@tamu.edu

Received 22 April 2018; Revised 2 July 2018; Accepted 17 July 2018; Published 23 August 2018

Academic Editor: Marco Rossi

Copyright © 2018 Alfredo D. Bobadilla et al. This is an open access article distributed under the Creative Commons Attribution License, which permits unrestricted use, distribution, and reproduction in any medium, provided the original work is properly cited.

Microelectronic fabrication of Si typically involves high-temperature or high-energy processes. For instance, wafer fabrication, transistor fabrication, and silicidation are all above 500°C. Contrary to that tradition, we believe low-energy processes constitute a better alternative to enable the industrial application of single-molecule devices based on 2D materials. The present work addresses the postsynthesis processing of graphene at unconventional low temperature, low energy, and low pressure in the poly methyl-methacrylate- (PMMA-) assisted transfer of graphene to oxide wafer, in the electron-beam lithography with PMMA, and in the plasma patterning of graphene with a PMMA ribbon mask. During the exposure to the oxygen plasma, unprotected areas of graphene are converted to graphene oxide. The exposure time required to produce the ribbon patterns on graphene is 2 minutes. We produce graphene ribbon patterns with ~50 nm width and integrate them into solid state and liquid gated transistor devices.

1. Introduction

Working with 2D materials such as graphene requires novel methods to fabricate ribbon patterns. Among the traditional methods are a metallic or resist mask to selectively protect graphene in plasma etch exposure [1–5] and focused ion-beam (FIB) etching [6, 7]. In an oxygen plasma at 200 mTorr and 50 Watts, the etch rate of graphene is about 1 layer per second [8], and a 5- to 10-second plasma etch exposure is typically employed to selectively etch graphene with a hydrogen silsesquioxane (HSQ) resist [8] or metallic mask [9]. At a shorter time (<4 seconds) of plasma etch exposure, graphene oxide can be generated [10]. Major drawbacks of the traditional methods are the lack of adaptability of FIB for mass production of devices, the usage of harsh acid treatment to remove the HSQ resist [5] or metal mask [9, 11], and overetching of graphene from the edges underneath the metallic ribbon mask [9]. With a HSQ ribbon mask, the resultant width of graphene ribbon pattern is ~10 nm smaller than the resist mask [8]. A polymethyl-methacrylate (PMMA) resist mask can also be employed to pattern graphene, and the edge roughness of the resultant pattern is ~5 nm [3]. The PMMA mask has been adopted in the fabrication of graphene constrictions or quantum dots [3,12–14] where they exploit the formation of "S" shaped edges, which is possibly due to the strong and normally undesired effect of etching from the edges. Despite its adoption to fabricate quantum dots, the PMMA resist mask has not been widely adopted to make patterns on graphene. A metallic mask is preferred instead of PMMA to make nanoscale patterns with widths or diameters smaller than 50 nm [9, 11, 15].

Novel methods to fabricate ribbon patterns include metallized DNA origami [16, 17], inorganic nanowire mask [18, 19], PMMA as sacrificial layer for a metallic mask [20, 21], and block-copolymer lithography [22, 23].

Major drawbacks of the novel methods are the lack of control on the creation of arbitrary patterns with block copolymer, obtaining sub-100 nm resolution with a PMMA sacrificial layer, and the lack of control of placement of a DNA nanostructure or nanowire on the graphene substrate.

On the other side, plasma etch exposure is also useful to reduce the number of layers in multilayer graphene down to single layer [24–27], to control the electronic bandgap of graphene by chemical functionalization [28, 29], and for controllably engineering atomically thin material systems with monolayer precision [30–32].

In the present work, novel parameters for plasma patterning of graphene/graphene oxide are identified to enable the usage of a PMMA ribbon mask cured at low temperature (<115°C). Low-temperature curing is unconventional in electron-beam lithography and PMMA typically shows low resistance to oxygen plasma etching [33]. PMMA is therefore normally considered inadequate as a mask for selective plasma etching at sub-50 nm resolution.

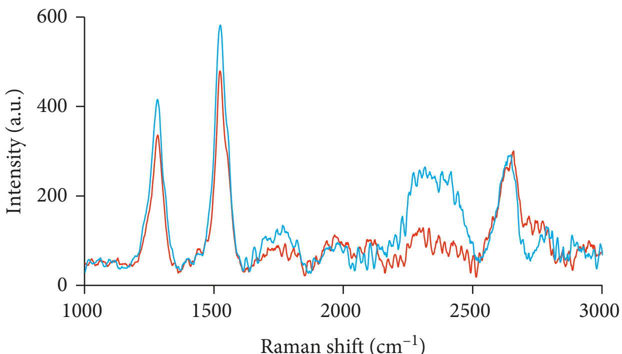

Figure 1: Two typical Raman characteristic (514 nm wavelength) of chemical vapor deposited (CVD) graphene with a high degree of disorder [37–39] on copper foil measured at two arbitrary points.

2. Materials and Methods

Graphene (Figure 1) was synthesized by chemical vapor deposition (CVD) on copper foil [34–36]. Impurities in the CVD chamber can be translated to the graphene sample, and thus, an oxygen plasma treatment of the chamber was completed before introducing the copper foil sample for CVD synthesis of graphene. Briefly, the CVD process began by annealing the copper foil at 800°C under a flow of hydrogen gas of 1000 sccm at 300 Torr for 30 minutes. Then, the temperature was set to 1000°C. When the temperature stabilized at 1000°C in all three monitored zones of the CVD furnace, hydrogen gas was purged at 0.1 Torr before exposing the copper foil to a flow of methane of 50 sccm at 1 Torr. In this process, graphene was deposited by the reduction of methane. After 3 minutes of methane flow, the gas was purged at 10 mTorr and the furnace heater was shut off to begin the cooling process. The cooling process was done initially under flows of hydrogen and argon of 1000 sccm each at 300 Torr for 5 minutes. For the rest of the cooling process (~75 minutes), only the hydrogen gas was kept active. The introduction of argon during the initial stages (5 minutes at 1000°C) of cooling yields a D peak (~1300 cm^{-1}) of increased intensity and a 2D peak (~2650 cm^{-1}) of reduced intensity in the Raman characteristics of graphene (Figure 1), which is consistent with reports of graphene with a high degree of disorder [37–39].

A PMMA (MicroChem) thin film, produced by spin coating, protected the front side of the graphene (a) during the etching of graphene on the backside of the copper foil in a dilute nitric acid solution (Table 1); (b) during the transfer of graphene to an oxide wafer (Table 2); and (c) during the oxygen plasma patterning of graphene ribbons on silicon dioxide (Figure 2).

The curing temperature of PMMA on graphene/copper foil and the temperature for drying of PMMA/graphene on the oxide wafer were either room temperature (21°C) in a vented hood (~12 hours) or 37°C on a hot plate (~3 hours).

After the transfer of graphene from the copper foil to an oxide wafer, we need to characterize the graphene through electrical measurements; this requires the fabrication of a graphene ribbon with electrodes, for which four lithography steps were implemented:

(a) Patterning on top of the oxide wafer (SiO_2/Si^{++}) and before graphene deposition by direct-write optical lithography (Microtech LW405) of back gate electrodes, as interface to the highly doped silicon (Si^{++}).

(b) Patterning of drain-source (D-S) electrodes and two auxiliary (Aux) electrodes after graphene deposition by optical lithography. Graphene covers most of the surface of the oxide wafer (~1 cm^2), and (D-S-Aux) electrodes were deposited on top of graphene. Back gate electrodes are employed for electrical measurements in air conditions. Auxiliary electrodes are employed as gate electrodes for electrical measurements in aqueous conditions.

(c) Etching away by a selective exposure to oxygen plasma with a photoresist mask of the areas surrounding the electrodes (except the zone between drain and source) to avoid electrical short circuit. Graphene has a good electrical conductivity and may cause short circuits between electrodes.

(d) Defining the ribbon pattern between drain and source electrodes by a selective exposure to oxygen plasma with a PMMA (e-beam resist) ribbon mask.

Electrodes were based on palladium, ~30 nm thick, and deposited by sputtering (AJA sputtering system). S1805 (MICROPOSIT S1800, film thickness ~0.5 μm) was chosen as photoresist; thicker resists left more residue impurities on graphene. The resist was spin coated at 3000 rpm for 30 seconds and cured at 90°C or 115°C for 1 minute. Acetone was employed as a resist remover in the liftoff process. 1165 solvent is the conventional remover of Shipley resists. However, we found that it causes detachment of graphene from the oxide substrate.

In order to perform the electron-beam (e-beam) lithography (Raith 150 e-beam system), the PMMA resist was cured on a hot plate and we tested three temperatures: room temperature (21°C for 12 hours), 37°C (3 hours), and 115°C (2 minutes). We did not observe significant differences in the outcome of the plasma etch due to the curing temperature of

Table 1: Process to remove chemical vapor deposited (CVD) graphene from the backside of copper foil by floating on a dilute nitric acid solution. A polymethyl-methacrylate (PMMA) thin film protects the front side of graphene/copper foil.

Step	Description
1	Spin coating of e-beam resist (PMMA A6) on one side of the graphene/copper foil/graphene at 3000 rpm for 1 minute
2	Curing of PMMA/graphene/copper/graphene either at 37°C for 3 hours on a hot plate or at room temperature (21°C) in a vented hood for 12 hours
3	Etching of graphene on the backside of PMMA/graphene/copper/graphene by floating on a solution of HNO_3/H_2O (1 : 10) for ~10–15 minutes
4	Rinsing of PMMA/graphene/copper by floating on distilled water for 3 minutes. Repeat three times the procedure
5	Drying of PMMA/graphene/copper foil with a nitrogen gun

Table 2: Process to transfer the PMMA/graphene from a copper foil to an oxide wafer. Transfer of the PMMA/graphene membrane between recipients is made with a silicon wafer.

Step	Description
1	Etch copper (backside of PMMA/graphene/copper) by floating on a diluted copper etchant/H_2O (1 : 10) solution for 12 hours
2	Rinse the PMMA/graphene by floating on distilled water for 2 minutes. Repeat five times the procedure
3	Rinse the PMMA/graphene by floating on a diluted HCl/H_2O (1 : 20) solution for 15 minutes [40]
4	Rinse the PMMA/graphene by floating on distilled water for 2 minutes. Repeat three times the procedure
5	Pick up the PMMA/graphene with an oxide (SiO_2/Si) wafer
6	Dry the PMMA/graphene/wafer either at 37°C for 3 hours on a hot plate or at room temperature (21°C) in a vented hood for 12 hours

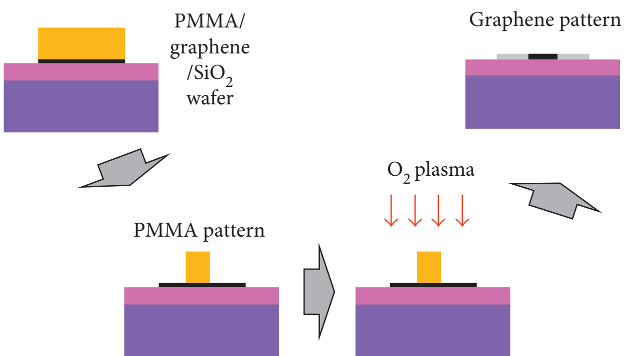

Figure 2: Patterning of graphene using a protective mask (PMMA) and exposure to oxygen plasma. Normally, PMMA shows poor resistance to oxygen plasma. The present work proposes novel physical processing parameters to enable the usage of PMMA as a mask to create ribbon patterns on graphene. Electron-beam (e-beam) lithography is used to create the PMMA mask.

PMMA resist. IPA/water (7 : 3) was used as the developer of PMMA [41–43] ribbon patterns at room temperature (21°C). The optimal development time of PMMA in IPA/water was different for different curing temperatures: ~10 s at room temperature, ~15 s at 37°C, and ~20 s at 115°C. We chose PMMA A2 950K, which originates films with ~60 nm thickness and therefore produces PMMA nanoribbons with good aspect ratio and stability since we need to fabricate nanoribbon patterns of width <100 nm. The optimal development time depends on the curing temperature, the chosen optimized e-beam dose parameters, and the resultant e-beam current during patterning.

Optimal parameters for the e-beam processing of PMMA nanoribbons on graphene included a high-voltage source of 30 kV, aperture of 10 μm, magnification of 2000, working distance of 10 mm, step size of 4 nm, area dwell time of 0.372 μs, and beam current of 34.38 pA. We test and suggest the following doses: 80, 100, and 120 $\mu C/cm^2$.

The graphene/PMMA ribbon mask was exposed to an oxygen plasma at low pressure (<40 mTorr) in a reactive ion etching (RIE) chamber (MARCH CS-1701) (Figure 2). Sometimes, there were delays of ~5–25 seconds in the activation of the plasma at low pressure. If the delay was longer, we turned off the plasma. Before reactivating the plasma, (a) we activated the vacuum pump to evacuate the gas; (b) set the oxygen gas pressure to 160 mTorr at 20 sccm; (c) activated again the vacuum pump to evacuate the gas; and (d) set the oxygen gas pressure to 30 mTorr at 1 sccm.

3. Results and Discussion

Polymer or metal masks are typically used to etch graphene. Physical vapor deposition of the metal mask inherently involves high-temperature molecular events and strong binding of the metal to graphene. Therefore, we opted for a PMMA-based mask, a polymeric material employed in e-beam lithography as a resist. However, PMMA is well known to have a very low resistance to plasma oxygen [33]. For example, a double layer of PMMA (PMMA 495K A2/PMMA 950K A4) can be employed to pattern a 65 nm width graphene ribbon [15], but a metallic mask is preferred to obtain smaller ribbons with widths smaller than 50 nm [9, 11, 15]. Therefore, different etch processing parameters are needed to enable PMMA as a nanoribbon mask for 50 nm or smaller widths. To find optimal parameters for the effective plasma patterning of a graphene nanoribbon, we analyze the events involved in the selective etching process of a 2D material. During the plasma etching process, at certain conditions of RF power and gas pressure, an atom of PMMA ejected at high kinetic energy can remove other PMMA atoms, this process constituting a chain reaction. The effect of this chain reaction on the material depends on the number of atoms of the material and, therefore, will have a stronger effect in the etching resistance of a 3D material (PMMA thin film) than in a 2D material (graphene). We suggest this is an important factor for which PMMA can show an etching resistance to oxygen plasma as poor as that of graphene. Therefore, to find conditions of improved etching resistance for PMMA and

for selective patterning of graphene, we should decrease the energy and the number of oxygen ions that initiate the chain reaction. Our aim was to find the lowest power, the lowest oxygen pressure, and the shortest time needed to etch graphene.

Firstly, we explored much lower levels of power to test the plasma etch resistance of graphene. We hypothesized that the strength of adhesion of graphene to the substrate can influence the etch resistance of graphene. We do not report the influence of different values of temperature (during graphene transfer or resist curing) on the resistance of graphene to plasma etching. However, we found that baking dry graphene/SiO_2 at 150°C or 180°C makes it significantly more difficult to remove graphene by exposure to oxygen plasma, so that higher power (>50 Watts) is needed to etch graphene. Working with temperature levels lower than 115°C at all stages of the fabrication process, graphene has a lower strength of adhesion to the oxide wafer and is easier to etch.

We found that 8 Watts is the minimum level of power needed to effectively pattern graphene in a reproducible way; at this level of power, our graphene sample on 300 nm thick SiO_2 becomes optically transparent after ~2 minutes of plasma exposure (oxygen, 20 sccm, 160 mTorr).

The next step is finding an adequate level of plasma pressure to optimize the etch resistance of PMMA. The lowest pressure at which the RIE instrument works is typically 40 mTorr, which is the level of pressure used to evacuate the gas present in the chamber before beginning a plasma etch process. However, by setting a lower pressure (30 mTorr) and a flow of gas oxygen of 1 sccm, we were still able to produce plasma. We found that the oxygen plasma produced at a minimum power of 8 Watts, 30 mTorr, and 1 sccm converts graphene to graphene oxide in two minutes. The structural change was noticeable by light microscopy and verified by Raman spectroscopy (Figure 3). An increase in the magnitude of the D peak (~1300 cm^{-1}), becoming larger than the G peak (1530 cm^{-1}), in the Raman characteristic of graphene ribbons (Figure 3) with respect to that of pristine graphene (Figure 1), agrees with previous reports on the patterning of graphene ribbons; that is, the increase in the D peak is obtained during the process of patterning [15, 44, 45].

After we found low power (8 Watts) and low pressure (~30 mTorr) parameters of oxygen plasma to effectively etch graphene, we needed testing the etching resistance of the PMMA ribbon masks on an oxide substrate (SiO_2) as well as on graphene/SiO_2. Thus, we fabricated PMMA ribbon masks of three different widths: 20, 50, and 100 nm. We were able to produce 20 nm width PMMA ribbons on an oxide substrate (Figure 4), but we were not able to produce them on graphene. We suggest, at very small width (20 nm), the PMMA ribbon mask detach from graphene during the development process. We were able to produce 50 nm (Figure 5) and 100 nm (not shown) width PMMA on an oxide substrate (SiO_2) as well as on graphene. Notice that the development process of PMMA nanoscale patterns is normally done at low temperature (−4°C) [46, 47]. However, in the present work, the development process was done at room temperature (21°C).

When PMMA is supported on SiO_2, all PMMA ribbon widths were able to withstand an exposure to the oxygen plasma (30 mTorr, 1 sccm, 8 Watts) for 2 minutes. By SEM (scanning electron microscopy), we did not observe a significant change in the width of PMMA ribbons after exposure to oxygen plasma at those conditions (Figure 4). Moreover, we found that 16 Watts is the minimum power needed to remove PMMA at 30 mTorr, 1 sccm, and 2 minutes.

Finally, when PMMA is supported on graphene/SiO_2, we tested the plasma etch (oxygen, 8 Watts, 30 mTorr, 2 min) with ribbon masks of 50 nm (Figures 5(a) and 5(b)) and 100 nm width (not shown) and characterized the resultant graphene ribbon patterns using SEM imaging (Raith 150 e-beam system) and electrical measurements (HP 4145A) (Figures 5(c)–5(f)).

The current-voltage (I_{ds}–V_g) characteristic at air conditions (Figure 5(e)) is similar to other reports of graphene ribbon electron devices. Han [8] reported a I_{max}/I_{min} value around ~1.6 ($V_g = 0$–$20\ V_{dc}$) for graphene ribbon with widths of 49 and 71 nm at 200 K. While Jeong et al. [45] reported a I_{max}/I_{min} value of ~3.1 ($V_g = 0$–$20\ V_{dc}$) for an array of graphene ribbons with sub-10 nm width at room temperature. In the present report, the I_{max}/I_{min} is around ~1.4 ($V_g = 0$–$20\ V_{dc}$) for graphene ribbons with width of 50 or 100 nm at room temperature. At lower temperature and smaller ribbon width, the I_{max}/I_{min} is expected to increase. For example, for a very small ribbon width of only 9 to 13 atoms width, the I_{max}/I_{min} is around ~1000 ($V_g = 0$–$20\ V_{dc}$) [48].

In the I_{ds}–V_g characteristic in water, the gate modulation is more effective (Figure 5(f)). An electric double layer formed at the interface of an aqueous solvent and graphene has been suggested as a dielectric that allows a more effective gate modulation of graphene [49–51]. The gate modulation in water solvent allows a I_{max}/I_{min} of ~2.2, similar to the one obtained in air ($V_g = -20$ to $+20\ V_{dc}$) but with a smaller gate voltage ($V_g = 0$ to $5\ V_{dc}$) applied.

4. Summary and Conclusions

A high-temperature treatment of the PMMA/graphene membrane can cause a poor or null yield of graphene transfer from the copper foil to the oxide wafer. We attribute this to a strong adhesion of PMMA to graphene, after curing on copper foil, and a shape memory effect of the polymer, which causes poor adhesion of the PMMA/graphene membrane to the oxide substrate during the drying process. We were able to overcome that obstacle with low-temperature curing of PMMA and low-temperature drying at 21 or 37°C. A low level of temperature for resist curing (<115°C) was also important to enable the usage of PMMA nanoribbons as a mask during the oxygen plasma patterning of graphene. Normally, under exposure to oxygen plasma, a PMMA nanoribbon mask degrades faster than graphene. We suggest the plasma etching process in a PMMA nanoribbon mask, a 3D material, is critically dependent on the effect of a chain reaction, and this effect is weaker when the plasma is set to low levels of pressure and energy. We showed that a low temperature of PMMA curing (<115°C)

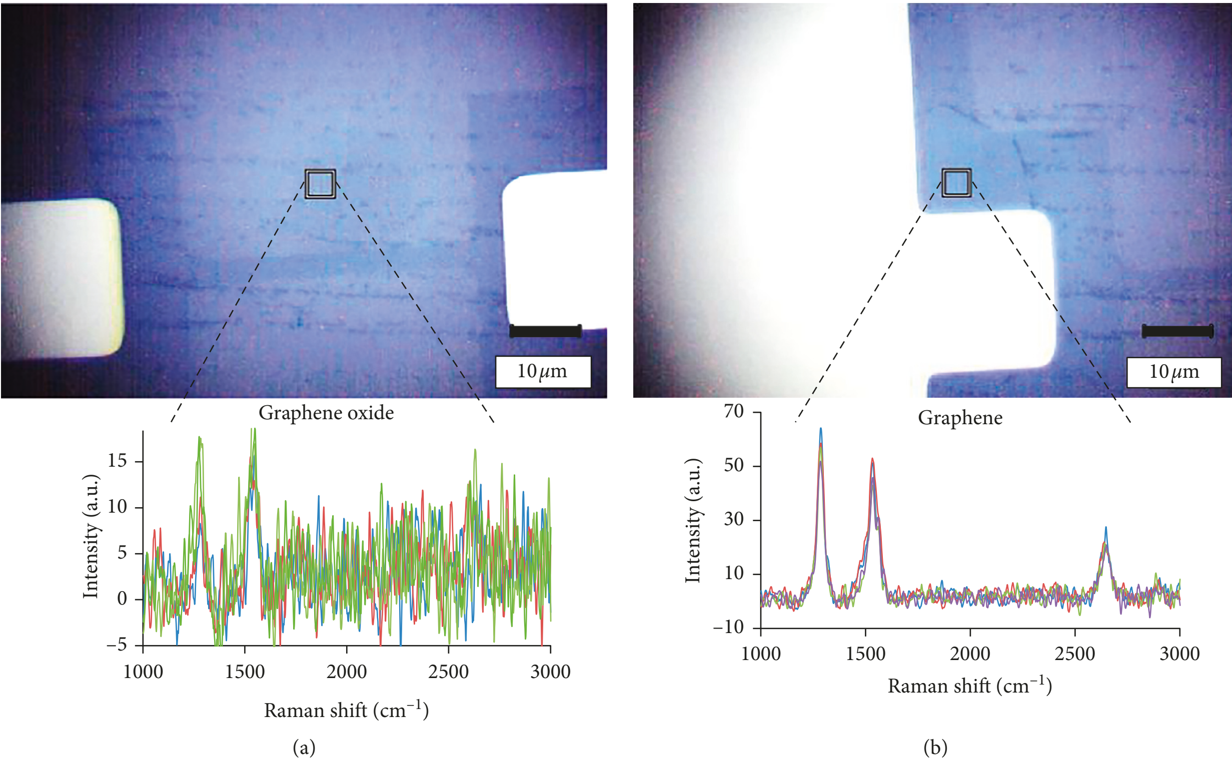

Figure 3: Raman characteristic (514 nm wavelength) of (a) graphene exposed to oxygen plasma (8 Watts, 30 mTorr, 1 sccm, 2 minutes) and (b) pristine graphene. The spectrum was measured on each corner point of a $(4\,\mu m)^2$ square area. The Raman characteristic of plasma-etched graphene corresponds to that of graphene oxide.

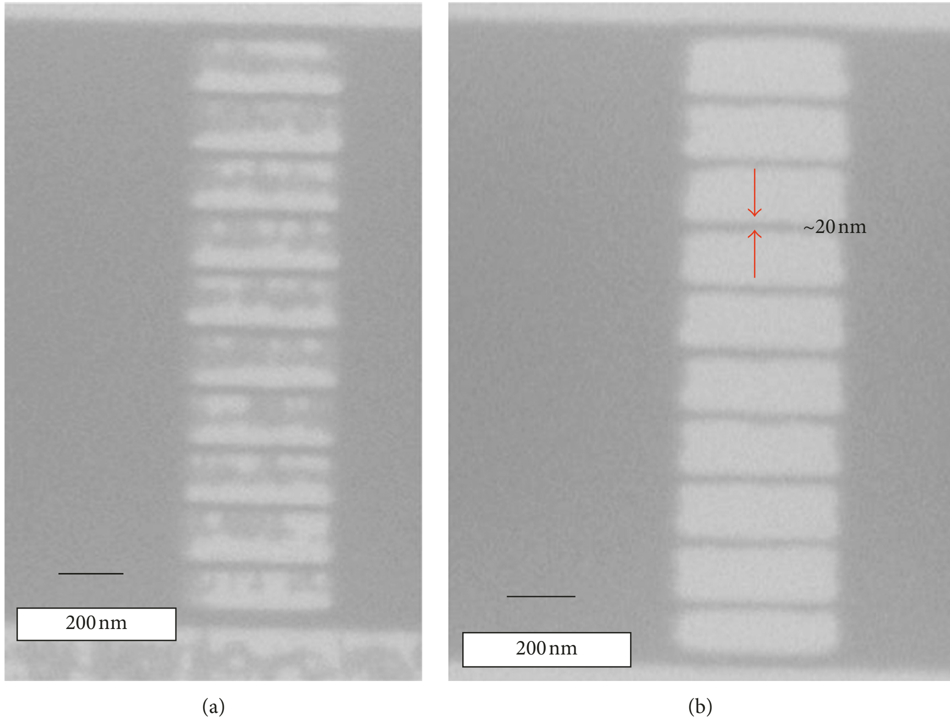

Figure 4: PMMA ribbon (~20 nm width) patterns on silicon dioxide (SiO_2) (a) before and (b) after exposure to oxygen plasma (8 Watts, 30 mTorr, 1 sccm, 2 minutes).

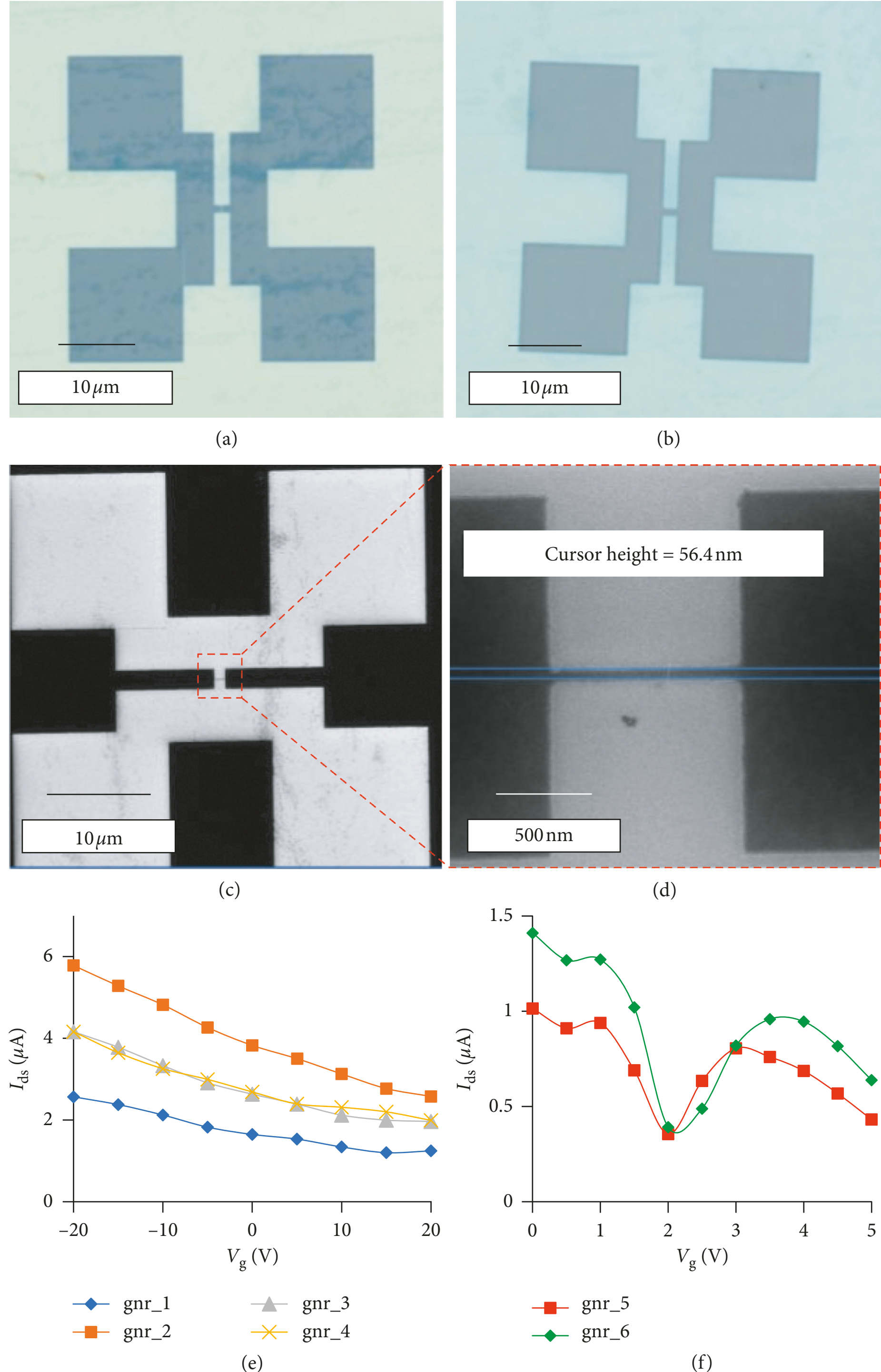

Figure 5: PMMA ribbon (~56 nm width) patterns on graphene/silicon dioxide (a) before and (b, c, d) after exposure to oxygen plasma (8 Watts, 30 mTorr, 1 sccm, 2 minutes). (a, b) Light microscope images. (c, d) Scanning electron microscope (SEM) images. Three-terminal electrical measurements (I_{ds}–V_g) are performed in different graphene nanoribbon ("gnr") devices in (e) air conditions and in (f) distilled water with a semiconductor analyzer. A backside gate electrode is used for measurements in air and a top gate electrode for measurements in water.

combined with low oxygen gas pressure (~30 mTorr) and low power (~8–12 Watts) produced ribbon patterns on graphene using a PMMA mask (~50 nm width, ~60 nm thick) in a reactive ion etching chamber (MARCH CS-1701). We did not analyze the role of intrinsic defects in the CVD graphene, which can play an important role in the plasma etch process. The method could be adapted to other types of polymer or UV resists. Other types of gases or chemical functionalization could also be explored to produce nanoribbon patterns on 2D materials.

Data Availability

The data used to support the findings of this study are included within the article.

Disclosure

The submitted manuscript has been created by UChicago Argonne, LLC, Operator of Argonne National Laboratory ("Argonne"). Argonne, a U.S. Department of Energy Office of Science laboratory, is operated under Contract DE-AC02-06CH11357. The U.S. Government retains for itself, and others acting on its behalf, a paid-up nonexclusive, irrevocable worldwide license in said article to reproduce, prepare derivative works, distribute copies to the public, and perform publicly and display publicly, by or on behalf of the government.

Conflicts of Interest

The authors declare no conflicts of interest exist.

Acknowledgments

The Center for Nanoscale Materials was supported by the U.S. Department of Energy, Office of Science, Office of Basic Energy Sciences, under Contract DE-AC02-06CH11357. The authors also acknowledge financial support from Argonne National Laboratory's Laboratory-Directed Research and Development Strategic Initiative.

References

[1] S. Kumar, N. Peltekis, K. Lee, H.-Y. Kim, and G. S. Duesberg, "Reliable processing of graphene using metal etchmasks," *Nanoscale Research Letters*, vol. 6, no. 1, p. 390, 2011.

[2] C. Lian, K. Tahy, T. Fang, G. Li, H. G. Xing, and D. Jena, "Quantum transport in graphene nanoribbons patterned by metal masks," *Applied Physics Letters*, vol. 96, no. 10, article 103109, 2010.

[3] L. Ponomarenko, F. Schedin, M. Katsnelson et al., "Chaotic Dirac billiard in graphene quantum dots," *Science*, vol. 320, no. 5874, pp. 356–358, 2008.

[4] Z. Chen, Y.-M. Lin, M. J. Rooks, and P. Avouris, "Graphene nano-ribbon electronics," *Physica E: Low-Dimensional Systems and Nanostructures*, vol. 40, no. 2, pp. 228–232, 2007.

[5] M. Y. Han, B. Özyilmaz, Y. Zhang, and P. Kim, "Energy band-gap engineering of graphene nanoribbons," *Physical Review Letters*, vol. 98, no. 20, article 206805, 2007.

[6] Z. Ye, H. Chao, S. Rujie et al., "A large-area 15 nm graphene nanoribbon array patterned by a focused ion beam," *Nanotechnology*, vol. 25, no. 13, article 135301, 2014.

[7] M. C. Lemme, D. C. Bell, J. R. Williams et al., "Etching of graphene devices with a helium ion beam," *ACS Nano*, vol. 3, no. 9, pp. 2674–2676, 2009.

[8] M. Y. Han, *Electronic transport in graphene nanoribbons*, Ph. D. doctoral dissertation, Physics, Columbia University, New York, NY, USA, 2010.

[9] A. Behnam, A. S. Lyons, M.-H. Bae et al., "Transport in nanoribbon interconnects obtained from graphene grown by chemical vapor deposition," *Nano Letters*, vol. 12, no. 9, pp. 4424–4430, 2012.

[10] I. Childres, L. A. Jauregui, J. Tian, and Y. P. Chen, "Effect of oxygen plasma etching on graphene studied using Raman spectroscopy and electronic transport measurements," *New Journal of Physics*, vol. 13, no. 2, article 025008, 2011.

[11] A. El Fatimy, R. L. Myers-Ward, A. K. Boyd, K. M. Daniels, D. K. Gaskill, and P. Barbara, "Epitaxial graphene quantum dots for high-performance terahertz bolometers," *Nature Nanotechnology*, vol. 11, no. 4, pp. 335–338, 2016.

[12] L.-J. Wang, G.-P. Guo, D. Wei et al., "Gates controlled parallel-coupled double quantum dot on both single layer and bilayer graphene," *Applied Physics Letters*, vol. 99, no. 11, article 112117, 2011.

[13] D. Wei, H.-O. Li, G. Cao et al., "Tuning inter-dot tunnel coupling of an etched graphene double quantum dot by adjacent metal gates," *Scientific Reports*, vol. 3, no. 1, p. 3175, 2013.

[14] X.-X. Song, H.-O. Li, J. You et al., "Suspending effect on low-frequency charge noise in graphene quantum dot," *Scientific Reports*, vol. 5, no. 1, p. 8142, 2015.

[15] M.-H. Bae, Z. Li, Z. Aksamija et al., "Ballistic to diffusive crossover of heat flow in graphene ribbons," *Nature Communications*, vol. 4, no. 1, p. 1734, 2013.

[16] Z. Jin, W. Sun, Y. Ke et al., "Metallized DNA nanolithography for encoding and transferring spatial information for graphene patterning," *Nature Communications*, vol. 4, no. 1, p. 1663, 2013.

[17] J. Choi, H. Chen, F. Li et al., "Nanomanufacturing of 2D transition metal dichalcogenide materials using self-assembled DNA nanotubes," *Small*, vol. 11, no. 41, pp. 5520–5527, 2015.

[18] J. Bai, X. Duan, and Y. Huang, "Rational fabrication of graphene nanoribbons using a nanowire etch mask," *Nano Letters*, vol. 9, no. 5, pp. 2083–2087, 2009.

[19] A. Sinitskii and J. M. Tour, "Patterning graphene nanoribbons using copper oxide nanowires," *Applied Physics Letters*, vol. 100, no. 10, article 103106, 2012.

[20] N. Kang, C. W. Smith, M. Ishigami, and S. I. Khondaker, "Simple patterning of large-area graphene by metal mask and sacrificial polymer layer," *ECS Meeting Abstracts*, vol. MA2014-01, p. 1262, 2014.

[21] T. Kaplas, A. Bera, A. Matikainen, P. Pääkkönen, and H. Lipsanen, "Transfer and patterning of chemical vapor deposited graphene by a multifunctional polymer film," *Applied Physics Letters*, vol. 112, no. 7, article 073107, 2018.

[22] J. G. Son, M. Son, K.-J. Moon et al., "Sub-10 nm graphene nanoribbon array field-effect transistors fabricated by block copolymer lithography," *Advanced Materials*, vol. 25, no. 34, pp. 4723–4728, 2013.

[23] H. S. Suh, D. H. Kim, P. Moni et al., "Sub-10-nm patterning via directed self-assembly of block copolymer films with a vapour-phase deposited topcoat," *Nature Nanotechnology*, vol. 12, no. 6, pp. 575–581, 2017.

[24] K. S. Hazra, J. Rafiee, M. A. Rafiee et al., "Thinning of multilayer graphene to monolayer graphene in a plasma environment," *Nanotechnology*, vol. 22, no. 2, article 025704, 2011.

[25] H. Al-Mumen, F. Rao, W. Li, and L. Dong, "Singular sheet etching of graphene with oxygen plasma," *Nano-Micro Letters*, vol. 6, no. 2, pp. 116–124, 2014.

[26] K. S. Kim, Y. J. Ji, Y. Nam et al., "Atomic layer etching of graphene through controlled ion beam for graphene-based electronics," *Scientific Reports*, vol. 7, no. 1, p. 2462, 2017.

[27] A. Davydova, E. Despiau-Pujo, G. Cunge, and D. B. Graves, "H+ ion-induced damage and etching of multilayer graphene

in H2 plasmas," *Journal of Applied Physics*, vol. 121, no. 13, article 133301, 2017.
[28] R. Balog, B. Jorgensen, L. Nilsson et al., "Bandgap opening in graphene induced by patterned hydrogen adsorption," *Nature Materials*, vol. 9, no. 4, pp. 315–319, 2010.
[29] A. Felten, A. Eckmann, J. J. Pireaux, R. Krupke, and C. Casiraghi, "Controlled modification of mono- and bilayer graphene in O_2, H_2 and CF_4 plasmas," *Nanotechnology*, vol. 24, no. 35, article 355705, 2013.
[30] G. Lee, J. Kim, K. Kim, and J. W. Han, "Precise control of defects in graphene using oxygen plasma," *Journal of Vacuum Science & Technology A*, vol. 33, article 060602, 2015.
[31] A. V. Jagtiani, H. Miyazoe, J. Chang et al., "Initial evaluation and comparison of plasma damage to atomic layer carbon materials using conventional and low Te plasma sources," *Journal of Vacuum Science & Technology A*, vol. 34, article 01B103, 2016.
[32] S. G. Walton, S. C. Hernández, D. R. Boris, T. B. Petrova, and G. M. Petrov, "Electron beam generated plasmas for the processing of graphene," *Journal of Physics D: Applied Physics*, vol. 50, no. 35, article 354001, 2017.
[33] D. J. Carbaugh, S. G. Pandya, J. T. Wright, S. Kaya, and F. Rahman, "Enhancing the dry etch resistance of polymethyl methacrylate patterned with electron beam lithography," *Journal of Vacuum Science & Technology B*, vol. 35, article 041602, 2017.
[34] R. Gulotty, S. Das, Y. Liu, and A. V. Sumant, "Effect of hydrogen flow during cooling phase to achieve uniform and repeatable growth of bilayer graphene on copper foils over large area," *Carbon*, vol. 77, pp. 341–350, 2014.
[35] I. Vlassiouk, M. Regmi, P. Fulvio et al., "Role of hydrogen in chemical vapor deposition growth of large single-crystal graphene," *ACS Nano*, vol. 5, no. 7, pp. 6069–6076, 2011.
[36] Z. R. Robinson, P. Tyagi, T. R. Mowll, C. A. Ventrice, and J. B. Hannon, "Argon-assisted growth of epitaxial graphene on Cu (111)," *Physical Review B*, vol. 86, no. 23, article 235413, 2012.
[37] E. H. Martins Ferreira, M. V. O. Moutinho, F. Stavale et al., "Evolution of the Raman spectra from single-, few-, and many-layer graphene with increasing disorder," *Physical Review B*, vol. 82, no. 12, article 125429, 2010.
[38] S. Claramunt, A. Varea, D. López-Díaz, M. M. Velázquez, A. Cornet, and A. Cirera, "The importance of interbands on the interpretation of the Raman spectrum of graphene oxide," *Journal of Physical Chemistry C*, vol. 119, no. 18, pp. 10123–10129, 2015.
[39] A. Eckmann, A. Felten, A. Mishchenko et al., "Probing the nature of defects in graphene by Raman spectroscopy," *Nano Letters*, vol. 12, no. 8, pp. 3925–3930, 2012.
[40] X. Liang, B. A. Sperling, I. Calizo et al., "Toward clean and crackless transfer of graphene," *ACS Nano*, vol. 5, no. 11, pp. 9144–9153, 2011.
[41] L. E. Ocola, "Development characteristics of PMMA in alternative alcohol:water mixtures," in *Proceedings of the APS March Meeting*, San Antonio, TX, USA, March 2015.
[42] S. Yasin, D. G. Hasko, and H. Ahmed, "Comparison of MIBK/IPA and water/IPA as PMMA developers for electron beam nanolithography," *Microelectronic Engineering*, vol. 61-62, pp. 745–753, 2002.
[43] S. Yasin, D. G. Hasko, and H. Ahmed, "Fabrication of <5 nm width lines in poly(methylmethacrylate) resist using a water: isopropyl alcohol developer and ultrasonically-assisted development," *Applied Physics Letters*, vol. 78, no. 18, pp. 2760–2762, 2001.
[44] A. Lyons, "Properties of graphene nanoribbons obtained by chemical vapor deposition," M.Sc., Electrical and Computer Engineering, University of Illinois at Urbana-Champaign, Champaign, IL, USA, 2012.
[45] S.-J. Jeong, S. Jo, J. Lee et al., "Self-aligned multichannel graphene nanoribbon transistor arrays fabricated at wafer scale," *Nano Letters*, vol. 16, no. 9, pp. 5378–5385, 2016.
[46] L. E. Ocola and A. Stein, "Effect of cold development on improvement in electron-beam nanopatterning resolution and line roughness," *Journal of Vacuum Science & Technology B: Microelectronics and Nanometer Structures*, vol. 24, no. 6, pp. 3061–3065, 2006.
[47] B. Cord, J. Lutkenhaus, and K. K. Berggren, "Optimal temperature for development of poly(methylmethacrylate)," *Journal of Vacuum Science & Technology B: Microelectronics and Nanometer Structures*, vol. 25, no. 6, pp. 2013–2016, 2007.
[48] J. P. Llinas, A. Fairbrother, G. B. Barin et al., "Short-channel field-effect transistors with 9-atom and 13-atom wide graphene nanoribbons," *Nature Communications*, vol. 8, no. 1, p. 633, 2017.
[49] J. Xia, F. Chen, J. Li, and N. Tao, "Measurement of the quantum capacitance of graphene," *Nature Nanotechnology*, vol. 4, no. 8, pp. 505–509, 2009.
[50] C. Reiner-Rozman, M. Larisika, C. Nowak, and W. Knoll, "Graphene-based liquid-gated field effect transistor for biosensing: Theory and experiments," *Biosensors and Bioelectronics*, vol. 70, pp. 21–27, 2015.
[51] A. D. Bobadilla, L. E. Ocola, A. V. Sumant, M. Kaminski, N. Kumar, and J. M. Seminario, "Europium effect on the electron transport in graphene ribbons," *Journal of Physical Chemistry C*, vol. 119, no. 39, pp. 22486–22495, 2015.

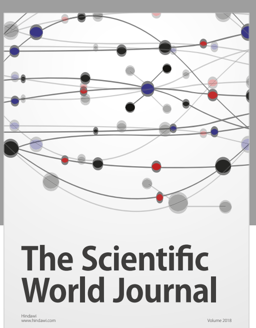

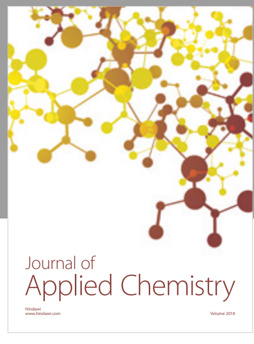

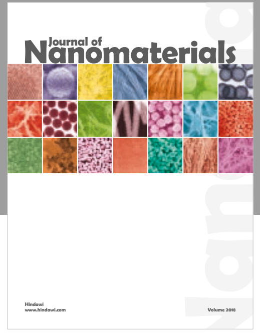

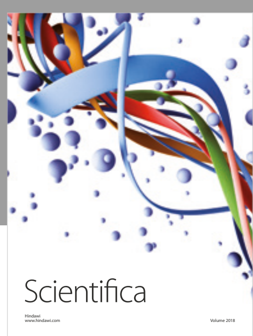

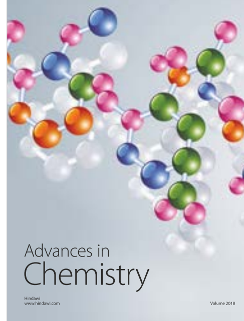

Submit your manuscripts at
www.hindawi.com